

A Passive Full-Wave Micromodeling Circuit for Packaging and Interconnection Problems

Yuhang Dou¹, Student Member, IEEE, and Ke-Li Wu¹, Fellow, IEEE

Abstract—A passive full-wave micromodeling circuit (FW-MMC) is proposed for high-speed/frequency interconnection problems. The circuit is derived from an FW generalized partial element equivalent circuit (G-PEEC) model, in which the radiation effect and other FW phenomena are fully taken into account. The proposed concise physically sensible circuit is obtained by recursively using a physics-based equivalent circuit transformation for absorbing the insignificant nodes of the G-PEEC model. To ensure the fidelity of the physical nature and the passivity of the MMC, the necessary broad sense criterion and the sufficient narrow sense criterion are systematically derived. It has been shown through numerical examples that the passivity violation of the physically sensible circuit model is very weak and can be effectively mediated. Thanks to the one order of magnitude reduction in the model order, the simulations for frequency- and time-domain system responses using the proposed MMC are three and two orders of magnitude faster, respectively, as compared with the G-PEEC model. Two practical examples for both frequency- and time-domains are given to demonstrate the high fidelity, scalability, accuracy, passivity, and efficiency of the FW-MMC.

Index Terms—Electromagnetic (EM), full-wave (FW), generalized partial element equivalent circuit (G-PEEC), model order reduction (MOR), signal integrity (SI).

I. INTRODUCTION

SIGNAL integrity (SI) issues have been becoming more and more crucial in high-speed/frequency electronic product designs to confront the high demands for high-performance computing (more than 100 Gb/s), cloud communication/computing (more than 50 Gb/s), and client devices (more than 20 Gb/s) [1]. A good SI design of interconnection and packaging circuits always ranks a high priority in a product development cycle, which usually could not be accomplished within a pressured time frame without an effective modeling tool for SI analysis. For a high-speed interconnection problem, various electromagnetic (EM) phenomena, such as radiation effect, mutual coupling, and material loss, become significant and must be taken into account. Furthermore, since

time-domain simulation must be concerned in the SI analysis, the simulation model must be ensured to be passive [2]. Therefore, to find a passive full-wave (FW) circuit model that is highly efficient for time-domain simulation is a long-lasting research theme in the EDA community.

Traditionally, the partial element equivalent circuit (PEEC) model has been intensively used in the SI analysis. The research on the PEEC model has been intensified in recent years in addressing many practical issues in electronic packaging design and EM radiation-related problems [3]–[7]. The PEEC model also has a good performance in solving many emerging EM problems, such as a graphene-based circuit, lighting transient analysis, and on-chip interconnect [8]–[15]. The PEEC model converts a multiconductor EM problem into a circuit model, which can theoretically incorporate external electric circuits or nonlinear elements and be solved by a SPICE-like circuit solver in both frequency- and time-domains. However, the mesh-based PEEC model consists of an excessively large number of partial elements for a practical interconnection problem, which takes a prohibitively long time for any practical SI analysis. In addition, it is difficult for designers to acquire the physical insight by examining its massy mesh-based partial elements.

In this work, an FW micromodeling method is proposed to derive a passive, concise, and physically sensible circuit model for high-speed interconnection and packaging problems. The micromodeling circuit (MMC) is derived from the frequency-domain FW generalized PEEC (G-PEEC) model [3], [7], which incorporates the radiation effect by complex-valued inductors while real-valued capacitors remain static. Compared with the PEEC model that incorporates the radiation effect by using complex-valued inductors and capacitors [8], the passivity violation of the G-PEEC model is minor and can be easily mediated.

The model order reduction (MOR) methods that are applicable to the PEEC model can be classified into two categories: macromodeling methods [16]–[22] and micromodeling methods [23]–[29]. A macromodeling method extracts a projection of a large-scale state-space system onto a lower dimensional subspace in a passband sense [16]–[18]. Some passivity enforcement methods for a macromodeling model have been proposed, including quadratic optimization [30] and Halmiltonian matrix perturbation [31]. For a high-speed wideband problem, multipoint-based approaches [19]–[21] have better performance on robustness and reliability than single-point

Manuscript received August 11, 2018; revised December 27, 2018 and February 14, 2019; accepted March 8, 2019. Date of publication April 22, 2019; date of current version June 4, 2019. This work was supported by the University Grants Committee of Hong Kong under Grant AoE/P-04/08. (Corresponding author: Ke-Li Wu.)

The authors are with the Department of Electronic Engineering, The Chinese University of Hong Kong, Hong Kong (e-mail: yhdou@link.cuhk.edu.hk; klwu@ee.cuhk.edu.hk).

Color versions of one or more of the figures in this paper are available online at <http://ieeexplore.ieee.org>.

Digital Object Identifier 10.1109/TMTT.2019.2909023

0018-9480 © 2019 IEEE. Personal use is permitted, but republication/redistribution requires IEEE permission. See http://www.ieee.org/publications_standards/publications/rights/index.html for more information.

interpolation approaches such as PRIMA [16]. The expansion points, which usually fall in the frequency band of interest, need to be determined carefully to avoid system poles that may cause severe approximation errors [21]. Since the expansion points and the order of expansion are not known *a priori*, a legitimate macromodeling model needs to be derived by an iterative procedure. Although the projected lower order state-space system can preserve the accuracy of the original model in the frequency band of interest, it lacks the direct physical interpretation of the original EM problem, and the passivity enforcement is quite mathematically involved.

On the other hand, a micromodeling method attempts to extract a circuit model with certain physical meanings, which is usually derived based on the node elimination or a circuit transformation. Some typical micromodeling methods include AMOR [23], TICER [24], SIP [25], and DPEC [26]. However, these methods have to use direct inductance proxy for mutual inductances, introducing a large number of redundant branches during node eliminating process and matrix inversions that limit the scalability. In addition, passivity is not guaranteed.

Recently, a static MMC (S-MMC) for a static PEEC model was proposed in [28] and [29] by the authors. It reduces the order of a static PEEC model by using a physics-based circuit transformation to absorb the insignificant nodes of the PEEC model one by one, recursively. The node absorbing process is systematic and stops automatically when the allowable accuracy criterion is no longer satisfied. The resultant concise circuit can be guaranteed to be passive using the passivity enforcement method proposed in [29]. The static micromodeling method in [29] does not involve any matrix inversions, and its derivation can be accelerated significantly by exploiting GPU parallel computation techniques [32], [33].

However, applying the quasi-static micromodeling method developed in [29] to the FW G-PEEC model directly leads to three disastrous problems.

- 1) Frequency-dependent complex-valued capacitances will be inevitably generated, which do not comply with the definition of capacitance and introduce severe passivity violation.
- 2) The stopping criterion for the quasi-static case is not applicable to the FW model because it is based on a low-pass approximation.
- 3) It is time-consuming in generating an FW-MMC at a high number of frequencies.

In this paper, an FW-MMC is proposed to accommodate these issues. Although the circuit transformation developed for the static case is adopted, a new updating formula of the circuit elements is developed. According to the new updating formula, the necessary broad sense and the sufficient narrow sense stopping criteria are systematically derived to ensure high fidelity of an FW circuit model. The frequency-dependent inductances and radiation resistances of the FW-MMC vary with frequency gradually and can be interpolated accurately by a few samples in the frequency band of interest with a pertinent circuit topology. In addition, the passivity of the circuit model can be guaranteed by the passivity enforcement scheme developed in [29]. For the resultant passive circuit with frequency-dependent elements, its time-domain response

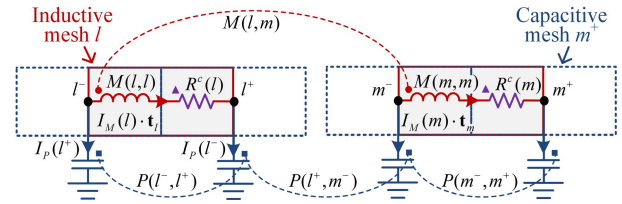


Fig. 1. Meshes and circuit interpretation of a G-PEEC model.

can be obtained efficiently by the transient analysis method proposed in [34] with guaranteed passivity and causality. Since the proposed MMC is usually one order of magnitude smaller than its original G-PEEC model, both the frequency- and time-domain simulation can be accelerated by about a thousand times.

To validate the effectiveness, accuracy, scalability, and the physical representation of the proposed FW-MMC, two numerical examples concerning an RF embedded bandpass filter and a multilayer interconnection circuit are given. Very good agreement between the results from the FW-MMC, the FW G-PEEC, and commercial EM software, showing the great potential of the proposed method for accurate circuit design and SI analysis, in which FW effects need to be taken into account. Limited by the G-PEEC model, the presented formula is applicable to large-scale multi-conductor EM problems in free space or layered dielectrics, in both frequency- and time-domains.

II. FULL-WAVE G-PEEC MODEL

The FW G-PEEC model is obtained from the FW mixed potential integral equation (MPIE), in which the radiation effect is accurately represented by self-radiation and mutual radiation resistances. It has been proven that the total radiation power dissipated by a self-radiation resistance of a short inductor cell of the G-PEEC model is identical to that of an electrically small dipole [3]. The conclusion on the radiated power has been further justified by Poynting's theorem [35]. For the sake of completeness, the G-PEEC model is briefly reviewed.

A. Partial Elements

The G-PEEC starts from the FW MPIE given by

$$\frac{\mathbf{J}(\mathbf{r})}{\sigma} = -\nabla \int_{v'} \frac{1}{\varepsilon_0} G(\mathbf{r}, \mathbf{r}') \rho(\mathbf{r}') dv' - j\omega \int_{v'} \mu_0 G(\mathbf{r}, \mathbf{r}') \cdot \mathbf{J}(\mathbf{r}') dv' \quad (1)$$

where ρ and \mathbf{J} are the volume charge and surface current densities, respectively, ω is the working frequency, and G is the FW Green's function for a particular boundary problem.

Discretizing the thin conductor surface using the well-known pulse function of the PEEC meshes shown in Fig. 1, applying Galerkin's matching procedure on an inductive mesh l and conflating the nonstatic portion of the (second term on the right-hand side (RHS) of (1) into the

first term leads to

$$R^c(l)I_M(l) + \sum_m j\omega M(l, m)I_M(m) + \sum_n \frac{1}{j\omega} [P(l^+, n) - P(l^-, n)]I_P(n) = 0 \quad (2)$$

where $I_M(l)$ is the conductive current on inductive mesh l flowing from node l^- to node l^+ and $I_P(n)$ is the displacement current flowing from node n to the ground, corresponding to the time derivative of the charge on capacitive mesh n . Partial resistance $R^c(l)$ is the conductor loss of inductive mesh l . Complex-valued $M(l, m)$ is the generalized partial inductance, which includes the radiation effects. Its real part and imaginary part correspond to the inductive coupling and radiation loss, respectively. The respective radiation resistance is embodied by $\text{Re}[j\omega M(l, m)]$. The partial coefficient of potential $P(l^\pm, n)$, which is called as potance in the context, represents capacitive coupling between capacitive meshes l^\pm and n . The general partial elements are given by

$$R^c(l) = l_l / \sigma a_l \quad (3)$$

$$P(l^\pm, n) = \frac{1}{\epsilon_0 v_{l^\pm} v_n} \int_{V_{l^\pm}} \int_{V_n} G_0(\mathbf{r}, \mathbf{r}') dv' dv \quad (4)$$

$$M(l, m) = \frac{\mu_0}{a_l a_m} \int_{V_l} \int_{V_m} (\mathbf{t}_l \cdot \mathbf{t}_m) G(\mathbf{r}, \mathbf{r}') dv' dv + [M'(l^-, m^+) - M'(l^-, m^-) - M'(l^+, m^+) + M'(l^+, m^-)] \quad (5)$$

$$M'(l^\pm, m^\pm) = \frac{1}{\omega^2 \epsilon_0 v_{l^\pm} v_{m^\pm}} \int_{V_{l^\pm}} \int_{V_{m^\pm}} [G(\mathbf{r}, \mathbf{r}') - G_0(\mathbf{r}, \mathbf{r}')] dv' dv \quad (6)$$

where a , v , and \mathbf{t} are the cross-sectional area, volume, and unit vector of the PEEC meshes, respectively. G_0 is static Green's function of the corresponding boundary problem. In the G-PEEC model, the resistors for conductor loss and the generalized inductors are frequency-dependent, whereas the potances are real-valued and frequency-independent. The circuit representation of Kirchhoff's voltage law (KVL) equation (2) is illustrated in Fig. 1. It needs to be pointed out that the ground in the G-PEEC model refers to the zero-potential reference at the infinity.

It will be shown through numerical examples that the passivity violation of a G-PEEC model is minor compared to that of the conventional FW PEEC model with complex-valued L and C [8]. The minor passivity violation is caused by numerical errors in dealing with very irregularly shaped meshes. Therefore, the passivity violation of the proposed FW-MMC will also be minor as it inherits the G-PEEC model. Nevertheless, the minor violation can be mediated by the passivity enforcement method proposed in [29]. Theoretically, the passivity of an FW circuit model is also frequency-dependent.

In the derivation of an FW-MMC, the complex-valued inductance matrix is denoted by \mathbf{M} , and the potance matrix is denoted by \mathbf{P} , both of which can be calculated directly. The resistances for conductor loss and the radiation resistances are conflated with the associated self-inductances and mutual

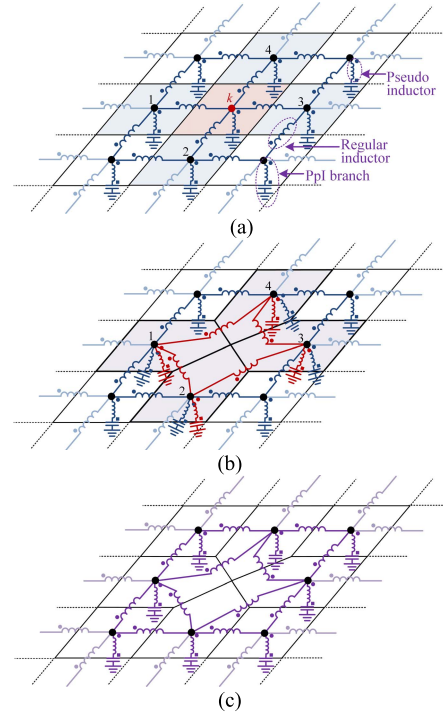


Fig. 2. Illustration of the node absorbing process. (a) Mesh and circuit topology of a G-PEEC model with generalized inductors and pseudoinductors. (b) Circuit transformation for absorbing node k . (c) The circuit with node k absorbed and shunt branches combined.

inductances for simplicity of expression. At the end of the micromodeling process, the resistances can be extracted from the imaginary parts of the inductances.

III. FULL-WAVE MICROMODELING CIRCUIT

The FW-MMC is derived by recursively utilizing the physics-inspired circuit transformation to absorb the insignificant nodes in an FW G-PEEC model. Although the node absorbing process has been introduced in [29] for a quasi-static PEEC model under low-pass approximation, it needs to be redeveloped for the FW micromodeling process in a bandpass sense to incorporate the radiation effect in the generalized inductances and preserve the static potances in each recursive iteration.

The circuit transformations for the node absorbing process are shown in Fig. 2. It is worth mentioning that a complex-valued pseudoinductor is introduced in series with each grounded potior in the G-PEEC model as shown in Fig. 2(a) to maintain a high fidelity of the micromodeling process.

The circuit transformation each time attempts to absorb one node by its neighboring nodes in accordance with the mesh rearrangement, which resembles the one shown in Fig. 2(a) to the one shown in Fig. 2(b). The transformation will introduce new inductors between its neighboring nodes defined on conductors and potior-pseudoinductor (PpI) branches between a node on a conductor and the ground. The elements updating formulas for an FW problem are the same as those for a quasi-static problem in form, which are given in [29, eqs. (16) and (18)] and therefore are not repeated here. After the circuit transformation, each newly generated PpI branch is combined

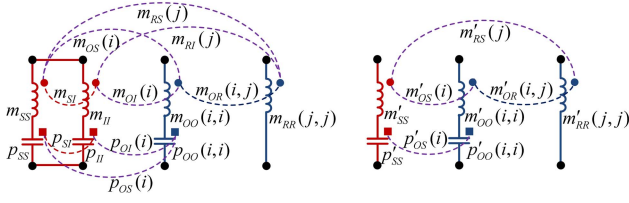


Fig. 3. Combining process of two coupled shunt PpI branches.

with the existing PpI branch and each newly introduced inductor is combined with the existing inductor, as shown in Fig. 2(c).

In Section III-A–III-C, theories for combining a pair of coupled shunt PpI branches, a physically sensible stopping criterion for the FW problem and a compact FW-MMC for a wide frequency band will be discussed in detail.

A. Combining Shunt PpI Branches

In an intermediate iteration during the micromodeling process, all the inductors and potors are coupled with all the elements of the same type through mutual inductances and mutual potances, respectively. As a result, combining a pair of coupled shunt PpI branches, as illustrated in Fig. 3, will affect the values of all the elements. To ensure that the updated potances remain to be real-valued, a legitimate updating formula needs to be derived. For the simplicity, the original inductance \mathbf{M} , potance \mathbf{P} , updated inductance \mathbf{M}' , and potance \mathbf{P}' are expressed in the form of block matrices as

$$\mathbf{M} = \begin{bmatrix} \mathbf{M}_{RR} & \mathbf{M}_{OR}^T & \mathbf{m}_{RS} & \mathbf{m}_{RI} \\ \mathbf{M}_{OR} & \mathbf{M}_{OO} & \mathbf{m}_{OS} & \mathbf{m}_{OI} \\ \mathbf{m}_{RS}^T & \mathbf{m}_{OS}^T & m_{SS} & m_{SI} \\ \mathbf{m}_{RI}^T & \mathbf{m}_{OI}^T & m_{SI} & m_{II} \end{bmatrix}$$

$$\mathbf{P} = \begin{bmatrix} \mathbf{P}_{OO} & \mathbf{p}_{OS} & \mathbf{p}_{OI} \\ \mathbf{p}_{OS}^T & p_{SS} & p_{SI} \\ \mathbf{p}_{OI}^T & p_{SI} & p_{II} \end{bmatrix}$$

$$\mathbf{M}' = \begin{bmatrix} \mathbf{M}'_{RR} & (\mathbf{M}'_{OR})^T & \mathbf{m}'_{RS} \\ \mathbf{M}'_{OR} & \mathbf{M}'_{OO} & \mathbf{m}'_{OS} \\ (\mathbf{m}'_{RS})^T & (\mathbf{m}'_{OS})^T & m'_{SS} \end{bmatrix}$$

$$\mathbf{P}' = \begin{bmatrix} \mathbf{P}'_{OO} & \mathbf{p}'_{OS} \\ (\mathbf{p}'_{OS})^T & p'_{SS} \end{bmatrix} \quad (7)$$

respectively, where subscripts I , S , O , and R represent the circuit elements in the newly introduced PpI branches, their shunt-connected PpI branches, other PpI branches, and the remaining inductor branches, respectively.

To combine two shunt branches, three equality conditions need to be satisfied.

- 1) The branch voltages remain the same.
- 2) The current through the combined branch equals the sum of the currents through the two shunt branches.
- 3) The currents through other branches remain the same.

With the equality conditions, the impedance equality formulas after combining a pair of shunt-connected PpI branches are

obtained in [29, eq. (23)], which are recited here for the sake of convenience

$$j\omega \mathbf{m}'_{SS} + \mathbf{p}'_{SS}/j\omega = j\omega k_1(e_5 - e_1 e_4 e_6 - \omega^2 e_7) + e_1 e_4/j\omega \quad (8)$$

$$j\omega \mathbf{m}'_{RS} = j\omega(k_2 \mathbf{m}_{RS} + k_3 \mathbf{m}_{RI}) \quad (9)$$

$$j\omega \mathbf{m}'_{OS} + \mathbf{p}'_{OS}/j\omega = j\omega(k_2 \mathbf{m}_{OS} + k_3 \mathbf{m}_{OI}) + (k_2 \mathbf{p}_{OS} + k_3 \mathbf{p}_{OI})/j\omega \quad (10)$$

$$j\omega \mathbf{M}'_{OO} + \mathbf{P}'_{OO}/j\omega = (\mathbf{P}_{OO} - k_1 \mathbf{p}_O \mathbf{p}_O^T)/j\omega + j\omega[\mathbf{M}_{OO} + k_1(\omega^2 \mathbf{m}_O \mathbf{m}_O^T - \mathbf{p}_O \mathbf{m}_O^T - \mathbf{m}_O \mathbf{p}_O^T)] \quad (11)$$

$$j\omega \mathbf{M}'_{OR} = j\omega[\mathbf{M}_{OR} + k_1(\omega^2 \mathbf{m}_O \mathbf{m}_R^T + \mathbf{p}_O \mathbf{m}_R^T)] \quad (12)$$

$$j\omega \mathbf{M}'_{RR} = j\omega[\mathbf{M}_{RR} + k_1(\omega^2 \mathbf{m}_R \mathbf{m}_R^T)] \quad (13)$$

where

$$\begin{aligned} e_1 &= 1/(p_{SS} + p_{II} - 2p_{SI}) \\ e_2 &= e_1(p_{II} - p_{SI}) \\ e_3 &= e_1(p_{SS} - p_{SI}) \\ e_4 &= p_{SS}p_{II} - (p_{SI})^2 \\ e_5 &= p_{II}m_{SS} + p_{SS}m_{II} - 2p_{SI}m_{SI} \\ e_6 &= m_{SS} + m_{II} - 2m_{SI} \\ e_7 &= m_{SS}m_{II} - (m_{SI})^2 \\ c_1 &= \omega^2(m_{SS} + m_{II} - 2m_{SI})/(p_{SS} + p_{II} - 2p_{SI}) \\ c_2 &= \omega^2(m_{II} - m_{SI})/(p_{II} - p_{SI}) \\ c_3 &= \omega^2(m_{SS} - m_{SI})/(p_{SS} - p_{SI}) \\ k_1 &= e_1/(1 - c_1) \\ k_2 &= e_2(1 - c_2)/(1 - c_1) \\ k_3 &= e_3(1 - c_3)/(1 - c_1) \\ \mathbf{m}_O &= \mathbf{m}_{OS} - \mathbf{m}_{OI} \\ \mathbf{m}_R &= \mathbf{m}_{RS} - \mathbf{m}_{RI} \\ \mathbf{p}_O &= \mathbf{p}_{OS} - \mathbf{p}_{OI}. \end{aligned} \quad (14)$$

The updating formulas for potances \mathbf{p}'_{OS} and \mathbf{P}'_{OO} used in the static method [29] is directly derived from impedance equality formulas (10) and (11), which is complex-valued and frequency-dependent for an FW circuit. The complex-valued and frequency-dependent potances will bring three issues.

- 1) *Lack of Physical Meaning*: Complex-valued and frequency-dependent potances do not comply with the physical meaning of the coefficient of potential, which is defined in a conservative electric field.
- 2) *Nonpassivity*: As the potances become complex-valued, the passivity violation of the resistance matrix associated with the real part of potances is very severe.
- 3) *Increase of Computational Overhead*: Introducing imaginary parts of potances will increase the order of the model by 30%. In addition, the frequency-dependent potances need to be calculated for each frequency, leading to a significant increase in computation time.

To find the real-valued potances, the RHS of (10) and (11) are rewritten as

$$\begin{aligned}
& j\omega(k_2\mathbf{m}_{OS} + k_3\mathbf{m}_{OI}) + (k_2\mathbf{p}_{OS} + k_3\mathbf{p}_{OI})/j\omega \\
&= j\omega(k_2\mathbf{m}_{OS} + k_3\mathbf{m}_{OI}) + (e_2\mathbf{p}_{OS} + e_3\mathbf{p}_{OI})/j\omega \\
&\quad + j\omega[(e_2 - k_2)/\omega^2\mathbf{p}_{OS} + (e_3 - k_3)/\omega^2\mathbf{p}_{OI}] \\
&(\mathbf{P}_{OO} - k_1\mathbf{p}_O\mathbf{p}_O^T)/j\omega \\
&= (\mathbf{P}_{OO} - e_1\mathbf{p}_O\mathbf{p}_O^T)/j\omega + j\omega(k_1 - e_1)\mathbf{p}_O\mathbf{p}_O^T/\omega^2 \\
&\quad + j\omega[\mathbf{M}_{OO} + k_1(\omega^2\mathbf{m}_O\mathbf{m}_O^T - \mathbf{p}_O\mathbf{m}_O^T - \mathbf{m}_O\mathbf{p}_O^T)] \quad (15)
\end{aligned}$$

respectively.

Substituting (15) and (16) into (10) and (11), real-valued coefficients for the $1/(j\omega)$ terms and complex-valued coefficients of the $j\omega$ terms in the revised (10) and (11) can be treated as real-valued potances and complex-valued inductances, respectively. By comparing the inductances and potances on both sides of (8)–(13), the updating formulas for the inductances and potances after combining the shunt PpI branches can be obtained as

$$\begin{aligned}
m'_{SS} &= k_1(e_5 - e_1e_4e_6 - \omega^2e_7) \\
\mathbf{m}'_{RS} &= k_2\mathbf{m}_{RS} + k_3\mathbf{m}_{RI} \\
\mathbf{m}'_{OS} &= k_2\mathbf{m}_{OS} + k_3\mathbf{m}_{OI} + \frac{e_2 - k_2}{\omega^2}\mathbf{p}_{OS} + \frac{e_3 - k_3}{\omega^2}\mathbf{p}_{OI} \\
\mathbf{M}'_{OO} &= \mathbf{M}_{OO} + k_1(\omega^2\mathbf{m}_O\mathbf{m}_O^T - \mathbf{m}_O\mathbf{p}_O^T - \mathbf{p}_O\mathbf{m}_O^T) \\
&\quad + (k_1 - e_1)\mathbf{p}_O\mathbf{p}_O^T/\omega^2 \\
\mathbf{M}'_{OR} &= \mathbf{M}_{OR} - k_1(\mathbf{p}_O\mathbf{m}_R^T - \omega^2\mathbf{m}_O\mathbf{m}_R^T) \\
\mathbf{M}'_{RR} &= \mathbf{M}_{RR} + \omega^2k_1\mathbf{m}_R\mathbf{m}_R^T \\
p'_{SS} &= e_1e_4 \\
\mathbf{p}'_{OS} &= e_2\mathbf{p}_{OS} + e_3\mathbf{p}_{OI} \\
\mathbf{P}'_{OO} &= \mathbf{P}_{OO} - e_1\mathbf{p}_O\mathbf{p}_O^T. \quad (17)
\end{aligned}$$

The updating formulas in (17) are compatible with the updating formulas for a quasi-static problem. When ω approaches 0, (17) degrades to those in [29, eq. (26)]. Since the original potances in an FW G-PEEC model are real-valued constants, coefficients e_1 , e_2 , e_3 , and e_4 are real-valued. Therefore, according to (17), the updated potances of the FW-MMC are real-valued constants, which comply with the fact that coefficients of potential are defined in a conservative electric field. As a side product, constant potances of an FW-MMC are frequency-independent and only need to be calculated once.

B. Stopping Criterion of Node Absorbing Process

The node absorbing process of the proposed micromodeling method is a recursive iteration process. It stops automatically when legitimate stopping criteria are no longer satisfied. The stopping criteria for the FW micromodeling method consist of a broad sense criterion and a narrow sense criterion.

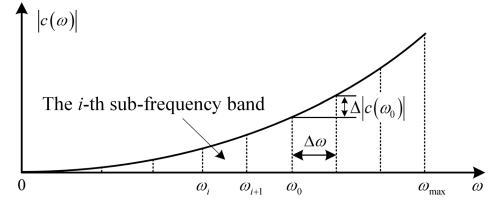


Fig. 4. Variation of $|c(\omega)|$ and definition of variation ripple in a subfrequency band.

1) *Stopping Criterion in a Broad Sense*: It has been shown that updating formulas in (17) depend on the frequency-dependent coefficients c_1 , c_2 , and c_3 . By physical intuition, for a physically sensible MMC, the variation rates of c_1 , c_2 , and c_3 versus frequency in a low-pass sense should not be too large. Denoting $|c(\omega)|$ as the maximum of $|c_1|$, $|c_2|$, and $|c_3|$, that is,

$$|c(\omega)| = \omega^2 \frac{|m_c|}{p_c} \quad (18)$$

where

$$\frac{|m_c|}{p_c} = \max\left(\frac{|m_{SS} + m_{II} - 2m_{SI}|}{p_{SS} + p_{II} - 2p_{SI}}, \frac{|m_{II} - m_{SI}|}{p_{II} - p_{SI}}, \frac{|m_{SS} - m_{SI}|}{p_{SS} - p_{SI}}\right). \quad (19)$$

The variation of $|c(\omega)|$ versus frequency should increase monotonically as illustrated in Fig. 4 although the inductances m_c also depend on the frequency. Therefore, $|c(\omega_{\max})|$ is the upper bound of $|c_1|$, $|c_2|$, and $|c_3|$ in a low-pass sense with cutoff frequency ω_{\max} . The upper bound $|c(\omega_{\max})|$ can be utilized to stipulate the micromodeling process in a broad sense. $|c(\omega_{\max})|$ must be set smaller than one for two reasons.

- 1) Stipulation of $|c(\omega_{\max})| < 1$ can prevent the updated inductances by (17) from being singular. When c_1 approaches 1, k_1 will approach infinity, which leads to some inductances, such as m'_{SS} in (17), approaching infinity.
- 2) Stipulation of $|c(\omega_{\max})| < 1$ can preserve the capacitive nature of the combined PpI branches. The PpI branches must be capacitive by nature. During the node-absorbing process, the inductances of pseudoinductors will increase, and potances will decrease. According to (18) and (19), when $|c(\omega_{\max})| = 1$ or > 1 , one of the two shunt PpI branches to be combined become resonant and even inductive.

In conclusion, the necessary broad sense stopping criterion is important to maintain the nature of the original G-PEEC circuit. The criterion only needs to be checked once at the cutoff frequency set forth by the user. An insignificant node can be absorbed only if its associated $|c(\omega_{\max})|$ is smaller than one.

2) *Stopping Criterion in a Narrow Sense*: Usually, an FW-MMC is generated pertinent to a narrow frequency band of interest, in which the variation of circuit elements is next to 0. To ensure the variation of the circuit element in a passband to be small, ripples of coefficients c_1 , c_2 , and c_3 in the passband must be small.

Assume that the frequency band of interest is $[\omega_0, \omega_0 + \Delta\omega]$ as shown in Fig. 4. The largest ripple of monotonic $|c(\omega)|$ in

the frequency band can be found to be

$$\begin{aligned} \Delta|c(\omega_0)| &= |c(\omega_0 + \Delta\omega)| - |c(\omega_0)| \\ &= (2\omega_0\Delta\omega + \Delta\omega^2) \frac{|mc|}{pc}. \end{aligned} \quad (20)$$

Therefore, the upper bound of ripples of c_1 , c_2 , and c_3 in the frequency band can be used as a criterion in a narrow sense for the micromodeling process. To generate an MMC that is effective in the vicinity of frequency ω_0 , only those insignificant nodes whose $\Delta|c(\omega_0)| < \delta$, where δ is a user prescribed bound of ripple, can be absorbed.

It has been shown that there are two stopping criteria for the micromodeling process, which are

$$|c(\omega_{\max})| < 1, \quad \text{in broad sense} \quad (21)$$

$$\Delta|c(\omega_0)| < \delta, \quad \text{in narrow sense.} \quad (22)$$

The criterion in a broad sense (21) stipulates the necessary condition for the FW micromodeling process. The criterion in the narrow sense (22) is a sufficient condition for controlling the variation of the elements to a frequency around frequency ω_0 . It is clear that the ripple bound $\Delta|c(\omega)|$ of coefficients c_1 , c_2 , and c_3 in a frequency band is proportional to the bandwidth and the frequency of interest.

Unlike the S-MMC presented in [29], which is a low-pass approximation with stopping criterion of $|c(\omega_{\max})| \ll 1$, the FW-MMC is a rigorous frequency-dependent circuit representation without any approximation error at each sampling frequency. The proposed broad and narrow sense stopping criteria are not used to control the accuracy but to control the passivity violation and element variation with respect to the frequency.

C. Full-Wave Micromodeling for A Wideband Problem

To generate a compact FW-MMC that is valid for a wide frequency band, it is advisable that the frequency band is divided into multiple subfrequency bands, as shown in Fig. 4. The MMC for each subfrequency band can be generated with the same circuit topology. Apparently, the ripple bound of the subfrequency band with the maximum operating frequency is the largest, and the number of nodes that can be absorbed for this subfrequency band is the smallest among all the subfrequency bands. Therefore, the topology of the MMC for the subfrequency band with the maximum operating frequency is derived first with the stopping criteria (21) and (22). Usually, the number of subfrequency bands depends on the overall bandwidth of interest and the allowable ripple bound. When the number of subfrequency bands is large, one needs to bear a heavy burden to derive the MMCs for all the subfrequency bands although they are in the same topology.

Taking the advantage that the generalized inductances in an MMC vary with frequency slowly in a wide frequency band and that the potances in an MMC are frequency-independent, it is not necessary to generate an MMC for every subfrequency band. As will be shown in the second numerical example, only the MMCs for a few subfrequency bands need to be generated. The generalized inductances for the rest of frequency points can be interpolated accurately while the potances are constant in all the subfrequency bands [36].

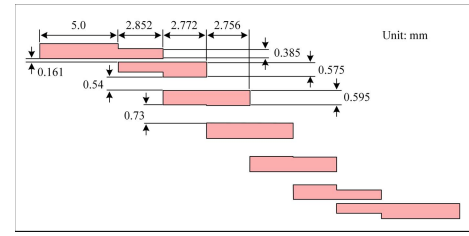


Fig. 5. Layout of the microstrip bandpass filter.

After the node absorbing process, three wrapping-up works need to be done to obtain a passive concise *RLP* circuit: 1) conflating the pseudoinductors by its surrounding regular inductors; 2) extracting the radiation resistors from the generalized inductors; and 3) enforcing the passivity of the MMC at each sampling frequency if needed. Procedures 1) and 3) are described in [29]. The frequency- and time-domain responses of the resultant circuit with frequency-dependent elements can be efficiently obtained by the SPICE-like solver using the modified nodal analysis (MNA) and the transient analysis method in [34], respectively.

IV. NUMERICAL EXAMPLES

In the following, two numerical examples are presented to validate the accuracy, compactness, scalability, and physical meaning of the proposed FW-MMC for high-speed/frequency problems. The first example is a wideband microstrip bandpass filter. It is used to demonstrate the accuracy and high fidelity of the proposed method in preserving the physical essence of an EM problem. The second example is a multilayer and multiport interconnection circuit, showing the accuracy, scalability, and efficiency for a wideband large-scale problem.

In all numerical examples, the G-PEEC models use the mixed rectangular and triangular meshing scheme and FW layered media Green's functions. The CPU and GPU modules used for computation are Intel i7 6700K and Nvidia Geforce GTX 980 Ti, respectively.

A. Microstrip Bandpass Filter

Fig. 5 shows the layout of the parallel-coupled half-wavelength resonator bandpass filter [38]. The substrate thickness is 0.635 mm with the relative permittivity of 10.2. The conductor thickness is 10 μm with the conductivity of $5.8 \times 10^7 \text{ S} \cdot \text{m}^{-1}$. An infinity large ground plane is assumed in the model.

The frequency band of the bandpass filter is 8–11 GHz. Therefore, the FW-MMC for the highest frequency 11 GHz is generated first. Then, the FW-MMCs with the same topology for other sampling frequencies are obtained. With the narrow sense stopping criterion δ set to 0.6, the FW-MMC for each sampling frequency contains only 56 self-potors and 81 self-inductors, whose circuit order is one order of magnitude less than that of its original model G-PEEC. Other details of the FW-MMC and the G-PEEC are compared in Table I, where the modeling time for the FW-MMC includes its respective G-PEEC generation time.

There are 31 sample frequency points in the frequency band. The S-parameters simulated by the FW-MMC and the

TABLE I
CIRCUIT DETAILS OF G-PEEC, FW-MMC, AND S-MMC

	G-PEEC	S-MMC	FW-MMC
No. of Potors	426	315	56
No. of Capacitive couplings	90,525	49,455	1,540
No. of Inductors	710	553	81
No. of Inductive couplings	251,695	152,628	3,240
Modeling time per frequency	11 secs	11+1 secs	11+3 secs

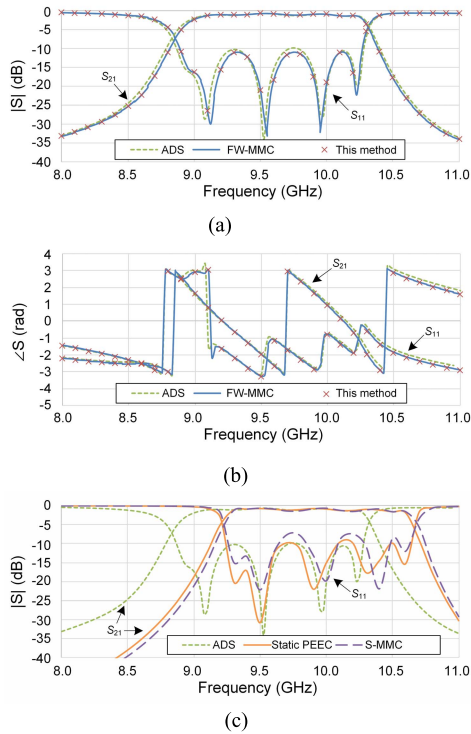


Fig. 6. S-parameters simulated by FW-MMC, G-PEEC, static PEEC, S-MMC, and ADS. (a) Magnitude of S-parameters. (b) Phase of S-parameters. (c) Magnitude of S-parameters simulated by static PEEC, S-MMC, and ADS.

G-PEEC are identical, as shown in Fig. 6(a) and (b), which match well with those simulated by ADS commercial software (RF momentum microwave module).

The proposed method is also compared with the S-MMC [29], which is derived from the static PEEC model [39] with the low-pass criterion of 0.01 and the maximum frequency of 11 GHz. The S-parameters obtained by the S-MMC and static PEEC have obvious deviation with those obtained by ADS, as observed from Fig. 6(c). Even though 315 nodes are used in the S-MMC, it cannot accurately approximate the response of its original static PEEC model in the high-frequency example. This predicament is overcome by the proposed FW-MMC.

For comparison purpose, the S-MMC is applied to the G-PEEC at 9.5 GHz with the low-pass criterion and the maximum frequency set to 0.1 and 11 GHz, respectively. The normalized passivity violation (NPV) factor, which is defined by the passivity violation factor [29] divided by the maximum positive eigenvalue of the element matrix,

TABLE II
NPVs OF G-PEEC, FW-MMC, AND S-MMC AT 9.5 GHz

Element matrix	G-PEEC model	FW-MMC	S-MMC
P	0	0	0
M	0	2.49×10^{-21}	1.16×10^{-15}
R in series with M	0	1.65×10^{-6}	9.06×10^{-5}
R in series with P	N/A	N/A	1.14

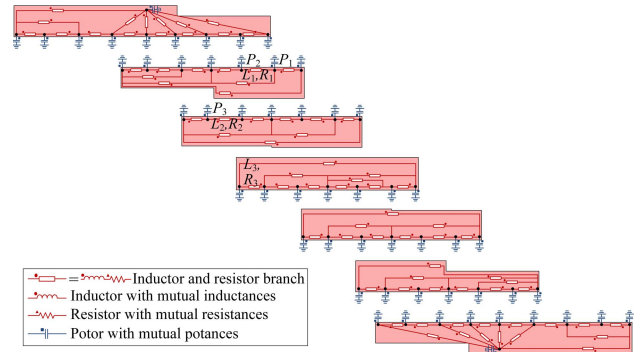


Fig. 7. FW-MMC topology of the bandpass filter. (Dimension is not in scale.)

is checked and compared with those of the proposed FW-MMC and its original model G-PEEC shown in Table II. It shows that the NPVs of potances, inductances, and resistances that are serially connected with inductances of FW-MMC and S-MMC are smaller than 1×10^{-4} , which can be remedied by the passivity enforcement. However, the NPV of the resistances that are serially connected with potances in the S-MMC is larger than 1, which is too severe to be remedied.

The FW-MMC of the bandpass filter is depicted in Fig. 7, which consists of radiation resistors (R), inductors (L), and potors (P). The mutual radiation resistances, mutual inductances, and mutual potances are represented by triangular dots, circular dots, and square dots, respectively. The circuit topology corresponds to the physical layout. Therefore, the inductive couplings, capacitive couplings, and radiation effect between different segments of the bandpass filter can be easily obtained. It is seen that the proposed FW-MMC can provide a clear physical insight into the EM problem.

The variation of the RLP element values in the frequency band is investigated. Fig. 8 shows the plots of some representative RLP element values that are labeled in Fig. 7. It can be observed from Fig. 8(a) that the potances are constant as expected, whereas inductances and radiation resistances are frequency-dependent but vary slowly and smoothly, as shown in Fig. 8(b) and (c), which can be easily interpolated by a three-order and five-order Newton polynomial functions [36] with four and six frequency samplings, respectively. By interpolating the circuit elements over a wide frequency band, a compact FW-MMC can be obtained.

In this example, the programs for generating the G-PEEC and the FW-MMC are executed by one core of the CPU module. The programs for S-parameter simulation and ADS are executed by four cores of the CPU in parallel.

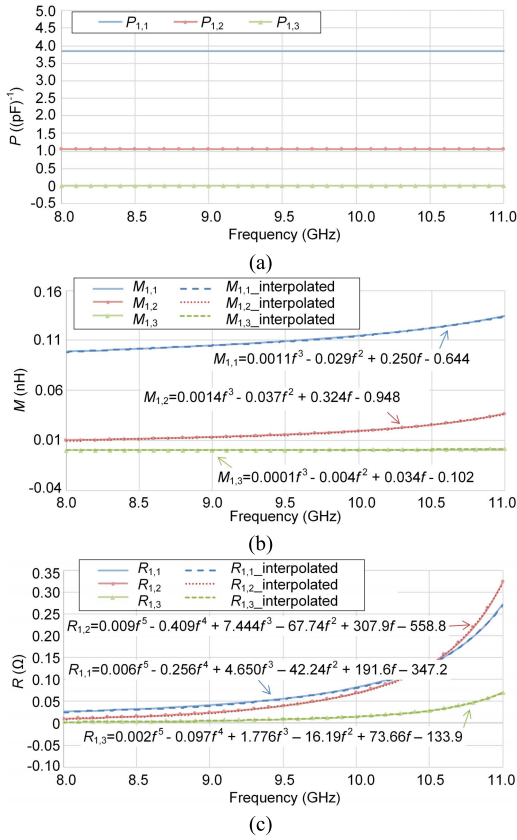


Fig. 8. Calculated and interpolated representative potances, inductances, and radiation resistances of the FW-MMC for the filter example. (a) Potances of $P_{1,1}$, $P_{1,2}$, and $P_{1,3}$. (b) Inductances $M_{1,1}$, $M_{1,2}$, and $M_{1,3}$. (c) Resistances of $R_{1,1}$, $R_{1,2}$, and $R_{1,3}$.

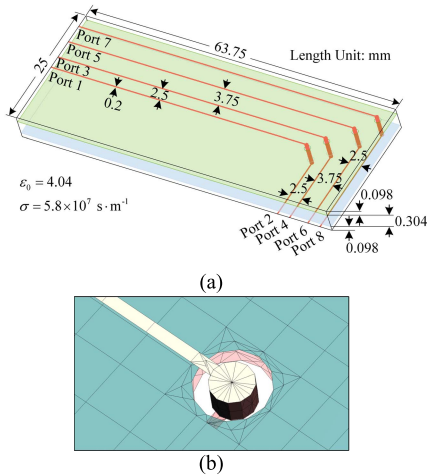


Fig. 9. Layout of the interconnection circuit. (a) Layout and dimension of the interconnection circuit. (b) Meshing scheme of one via.

B. Multilayer Interconnection Circuit

This example is to show the scalability of the proposed FW-MMC for a large-scale interconnection problem. To this end, a four-layer interconnection circuit illustrated in Fig. 9(a) is chosen to validate the effectiveness, accuracy, and passivity of the proposed method for a large-scale problem.

TABLE III
COMPARISON OF G-PEEC AND FW-MMC

	G-PEEC model	FW-MMC
No. of Potors	7,711	822
No. of Capacitive couplings	29,725,905	33,7431
No. of Inductors	14,457	1,755
No. of Inductive couplings	104,495,196	1,539,135
Generation time per frequency	7 min 11 s	7 min 11 s + 9 min 13 s
Total modeling time per frequency	7 min 11 s	7 min 11 s + 9 min 13 s
Simulation time for S-parameters (120 frequency points)	1,473 min 52 s	3 min 40 s
Average relative error of $ S_{11} $, $ S_{12} $	N/A	0.15% / 0.56%
Average error of $\angle S_{11}$ and $\angle S_{12}$	N/A	0.005 rad / 0.001 rad
Simulation time for S-parameters using HFSS:		963 min 20 s
Modeling time of PRIMA per frequency:		7 min 11 s + 137 min 30 s

The interconnection circuit consists of four signal traces on the top and bottom layers, which are connected through via holes. The surfaces of the conductor vias are meshed as shown in Fig. 9(b). The overall dimensions of the circuit are $63.75 \times 25 \times 0.5 \text{ mm}^3$. The metal thickness is set to $10 \mu\text{m}$, the metal conductivity is $5.8 \times 10^7 \text{ S}\cdot\text{m}^{-1}$, and the relative dielectric constant is 4.04.

Having had the two power plates, in the G-PEEC, there are 7711 coupled potors and 14457 coupled inductors. The simulation time for the S-parameters using the G-PEEC is 1473 min 52 s. As a reference, the simulation by HFSS takes 963 min 20 s. In applying the FW-MMC to this wideband large-scale problem, only seven frequency points (i.e., 0.1, 2, 4, 6, 8, 10, and 12 GHz) are needed. The FW-MMC at the highest frequency of 12 GHz is generated first, while the narrow sense stopping criterion δ is set to 0.05. The FW-MMCs at other sampling frequency points are obtained using the same circuit topology. Finally, the FW-MMCs at other frequency points are interpolated by a fourth-order Newton interpolation. The resultant circuit only consists of 822 coupled potors and 1755 coupled inductors. Using the FW-MMC, the simulation time for the S-parameters is reduced to 3 min 40 s. The details of the G-PEEC and the FW-MMC are compared in Table III, where the time for obtaining the FW-MMC includes the time for generating its respective G-PEEC.

The simulated S-parameters by FW-MMC, G-PEEC, and HFSS are compared in Fig. 10. The average errors of $|S_{11}|$ and $|S_{12}|$ simulated by the interpolated FW-MMC compared to those by G-PEEC are 0.15% and 0.56%, respectively, across the whole band. As shown in Fig. 10(c) and (d), the phases of S_{11} and S_{12} simulated by the G-PEEC and the FW-MMC also match well. The average errors in S_{11} and S_{12} phases are 0.005 and 0.001 rad, respectively.

The NPVs of the G-PEEC, the FW-MMC and the FW PEEC models [15] with complex-valued LC generated at 6 GHz are compared in Table IV. For both the G-PEEC and the FW-MMC, the NPV of the \mathbf{M} matrix and \mathbf{R} matrix are smaller than 10^{-3} , which can be mediated to be passive using the passivity enforcement method in [29]. However, the NPV of the \mathbf{R} matrix extracted from potors of the complex-valued LC

TABLE IV
NPVs of PEEC, G-PEEC, and FW-MMC at 6 GHz

Element matrix	PEEC model	G-PEEC model	This method
P	0	0	0
M	0	1.52×10^{-5}	4.05×10^{-4}
R in series with M	0	3.36×10^{-5}	1.45×10^{-4}
R in series with P	0.612	N/A	N/A
Time of passivity enforcement	N/A	1,388 min 29 s	1 min 32 s

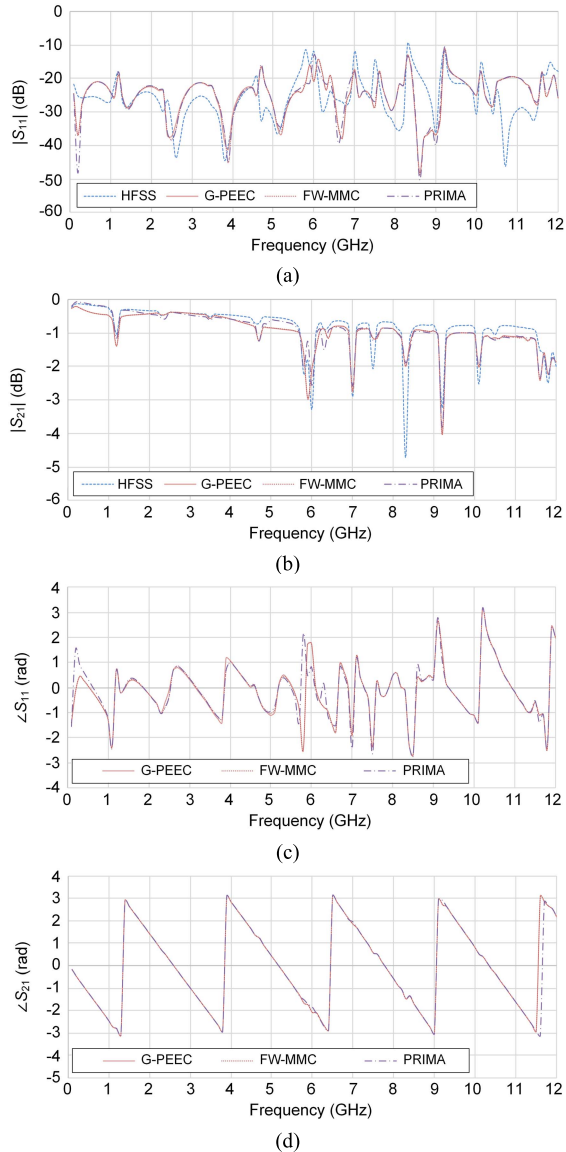


Fig. 10. Simulated S-parameters obtained by FW-MMC, G-PEEC, and HFSS. (a) Magnitude of S_{11} . (b) Magnitude of S_{21} . (c) Phase of S_{11} . (d) Phase of S_{21} .

PEEC model is 0.612, which is too large to be mediated. The time for passivity enforcement of the G-PEEC and the proposed FW-MMC are 1388 min 29 s and 1 min 32 s, respectively.

The derivation time for an FW-MMC is an important issue to be considered. The computational overhead of the

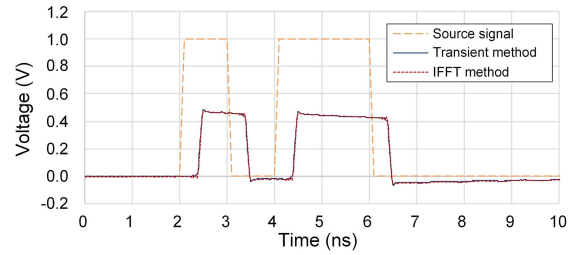


Fig. 11. Source signal and time-domain response of the FW-MMC at port 2 when port 1 is excited by transient analysis method [34] and the IFFT method.

micromodeling process is $O(n^3)$. However, the derivation of the FW-MMC can be accelerated by the parallel computation technique using GPUs, because its dominant operation is an outer product of two vectors. For this interconnection problem, the computation time of the FW-MMC for one frequency point is 9 min 13 s, which is accelerated by 30 times by a GPU module [32], [33].

The S-parameters obtained by the PRIMA model are also shown in Fig. 10. Since the PRIMA method needs matrix inversions and QR decompositions, its scalability is a major concern, and its computational overhead is high. In this example, the PRIMA process time for the G-PEEC per frequency is 137 min 30 s. On the other hand, the proposed FW-MMC does not involve any matrix inversions or decompositions, and its generation can be accelerated easily by GPU parallel computation techniques. In this example, the proposed method only costs 9 min 13 s per frequency by using the GPU module, not mentioning that the PRIMA model does not provide any intermediate physical interpretation.

To demonstrate the superiority of the proposed FW-MMC for time-domain simulation, the time-domain simulation of the FW-MMC of the interconnection circuit is also conducted using the transient analysis method proposed in [34]. The output responses at all the ports can be obtained in one run when port 1 is excited. The source signal is a pulse signal with 1-ns pulsewidth and is shown in Fig. 11. Only the time-domain output response at port 2 is presented in Fig. 11. It is shown that the simulated response is stable. For a fair comparison on computing time, the time-domain result is compared with that of the FW-MMC model but obtained by the conventional IFFT method shown in Fig. 11. With the same time interval, the simulation times by using the method in [34] and the IFFT method are 23 min 14 s and 44 min 3 s, respectively. The simulation result of the G-PEEC model using the IFFT method is not provided because the simulation time is prohibitively long, and the result is the same as that of FW-MMC. Based on the order of the G-PEEC model, the estimated simulation time for the time-domain response based on the G-PEEC model by the method in [34] and IFFT would be about 1250 and 16214 min, respectively.

In this example, the programs for the G-PEEC are executed by one core of the CPU module. The programs for S-parameter simulation and HFSS are executed by the four cores of the CPU module. The FW-MMC process is executed by the GPU module.

V. CONCLUSION

This paper presents a passive physics-based FW-MMC that can accurately describe not only the inductive and capacitive couplings but also the radiation effect in a large-scale high-speed interconnection and packaging problem. The derivation of the concise circuit does not involve any matrix inversions or decompositions, which can be highly accelerated by GPU parallel computation. For a wideband problem, the compact FW-MMC can be obtained by interpolating the circuit element values at a few sampling frequency points. The broad sense necessary condition and the narrow sense sufficient condition that ensure the fundamental physical nature and the element variation of the MMC are systematically derived. With the proposed MMC, the simulation time for system responses in the frequency- and time-domain simulations can be reduced by about three and two orders of magnitude compared to that if a G-PEEC model is used, respectively. Two numerical examples in both frequency- and time-domain are given to demonstrate the versatility, scalability, accuracy, passivity, and simplicity of the proposed MMC through the comparisons with the G-PEEC model and commercial EM software. It has demonstrated that the proposed method has a high potential for efficient and effective simulation of a large-scale interconnection and packaging problem.

REFERENCES

- [1] T.-L. Wu, F. Buesink, and F. Canavero, "Overview of signal integrity and EMC design technologies on PCB: Fundamentals and latest progress," *IEEE Trans. Electromagn. Compat.*, vol. 55, no. 4, pp. 624–638, Aug. 2013.
- [2] P. Triverio, S. Grivet-Talocia, M. S. Nakhla, F. G. Canavero, and R. Achar, "Stability, causality, and passivity in electrical interconnect models," *IEEE Trans. Adv. Packag.*, vol. 30, no. 4, pp. 795–808, Nov. 2007.
- [3] L. K. Yeung and K.-L. Wu, "Generalized partial element equivalent circuit (PEEC) modeling with radiation effect," *IEEE Trans. Microw. Theory Techn.*, vol. 59, no. 10, pp. 2377–2384, Oct. 2011.
- [4] B. P. Nayak, S. R. Vedicherla, and D. Gope, "Nonorthogonal 2.5-D PEEC for power integrity analysis of package-board geometries," *IEEE Trans. Microw. Theory Techn.*, vol. 65, no. 4, pp. 1203–1214, Apr. 2017.
- [5] J. Park, L. Lee, B. Seol, and J. Kim, "Fast and accurate calculation of system-level ESD noise coupling to a signal trace by PEEC model decomposition," *IEEE Trans. Microw. Theory Techn.*, vol. 65, no. 1, pp. 50–61, Jan. 2017.
- [6] L. Wei *et al.*, "Plane-pair PEEC model for power distribution networks with sub-meshing techniques," *IEEE Trans. Microw. Theory Techn.*, vol. 64, no. 3, pp. 733–741, Mar. 2017.
- [7] L. K. Yeung and K.-L. Wu, "PEEC modeling of radiation problems for microstrip structures," *IEEE Trans. Antennas Propag.*, vol. 61, no. 7, pp. 3648–3655, Jul. 2013.
- [8] Y. S. Cao, L. J. Jiang, and A. E. Ruehli, "Distributive radiation and transfer characterization based on the PEEC method," *IEEE Trans. Electromagn. Compat.*, vol. 57, no. 4, pp. 734–742, Aug. 2015.
- [9] D. Romano and G. Antonini, "Partial element equivalent circuit-based transient analysis of graphene-based interconnects," *IEEE Trans. Electromagn. Compat.*, vol. 58, no. 3, pp. 801–810, Jun. 2016.
- [10] W.-S. Zhao *et al.*, "High-frequency modeling of on-chip coupled carbon nanotube interconnects for millimeter-wave applications," *IEEE Trans. Compon., Packag., Manuf. Technol.*, vol. 6, no. 8, pp. 1226–1232, Aug. 2016.
- [11] M. Bandinelli *et al.*, "A surface PEEC formulation for high-fidelity analysis of the current return networks in composite aircrafts," *IEEE Trans. Electromagn. Compat.*, vol. 57, no. 5, pp. 1027–1036, Oct. 2015.
- [12] H. Chen, Y. Du, and M. Chen, "Lightning transient analysis of radio base stations," *IEEE Trans. Power Del.*, vol. 33, no. 5, pp. 2187–2197, Oct. 2018.
- [13] A. Rong, A. C. Cangellaris, and L. Dong, "Comprehensive broadband electromagnetic modeling of on-chip interconnects with a surface discretization-based generalized PEEC model," *IEEE Trans. Adv. Packag.*, vol. 28, no. 3, pp. 434–444, Aug. 2005.
- [14] I. F. Kovačević, T. Friedli, A. M. Müsing, and J. W. Kolar, "3-D electromagnetic modeling of parasitics and mutual coupling in EMI filters," *IEEE Trans. Power Electron.*, vol. 29, no. 1, pp. 135–149, Jan. 2014.
- [15] Y. S. Cao, L. J. Jiang, and A. E. Ruehli, "An equivalent circuit model for graphene-based terahertz antenna using the PEEC method," *IEEE Trans. Antennas Propag.*, vol. 64, no. 4, pp. 1385–1393, Apr. 2016.
- [16] A. Odabasioglu, M. Celik, and L. T. Pileggi, "PRIMA: Passive reduced-order interconnect macromodeling algorithm," *IEEE Trans. Comput.-Aided Design Integr. Circuits Syst.*, vol. 17, no. 8, pp. 645–654, Aug. 1998.
- [17] F. Ferranti, G. Antonini, T. Dhaene, and L. Knockaert, "Guaranteed passive parameterized model order reduction of the partial element equivalent circuit (PEEC) method," *IEEE Trans. Electromagn. Compat.*, vol. 52, no. 4, pp. 974–984, Nov. 2010.
- [18] R. W. Freund, "Model reduction methods based on Krylov subspaces," *Acta Numerica*, vol. 12, pp. 267–319, Jul. 2013.
- [19] F. Ferranti, M. S. Nakhla, G. Antonini, T. Dhaene, L. Knockaert, and A. E. Ruehli, "Multipoint full-wave model order reduction for delayed PEEC models with large delays," *IEEE Trans. Electromagn. Compat.*, vol. 53, no. 4, pp. 959–967, Nov. 2011.
- [20] L. Feng, J. G. Korvink, and P. Benner, "A fully adaptive scheme for model order reduction based on moment matching," *IEEE Trans. Compon., Packag., Manuf. Technol.*, vol. 5, no. 12, pp. 1872–1884, Dec. 2015.
- [21] T. Nguyen, T. L. Duc, T. Tran, J. Guichon, O. Chadebec, and G. Meunier, "Adaptive multipoint model order reduction scheme for large-scale inductive PEEC circuits," *IEEE Trans. Electromagn. Compat.*, vol. 59, no. 4, pp. 1143–1151, Aug. 2017.
- [22] S. Grivet-Talocia and B. Gustavsen, "Macromodeling via model order reduction," in *Passive Macromodeling: Theory and Applications*, 1st ed. Hoboken, NJ, USA: Wiley, 2016, ch. 5, pp. 135–165.
- [23] Y. Su, F. Yang, and X. Zeng, "AMOR: An efficient aggregating based model order reduction method for many-terminal interconnect circuits," in *Proc. Design Autom. Conf.*, San Francisco, CA, USA, 2012, pp. 295–300.
- [24] C. S. Amin, M. H. Chowdhury, and Y. I. Ismail, "Realizable reduction of interconnect circuits including self and mutual inductances," *IEEE Trans. Comput.-Aided Design Integr. Circuits Syst.*, vol. 24, no. 2, pp. 271–277, Feb. 2005.
- [25] Z. Ye, D. Vasilyev, Z. Zhu, and J. R. Phillips, "Sparse implicit projection (SIP) for reduction of general many-terminal networks," in *Proc. IEEE/ACM Int. Conf. Comput.-Aided Design*, San Francisco, CA, USA, Nov. 2008, pp. 736–743.
- [26] J. Wang and K.-L. Wu, "A derived physically expressive circuit model for multilayer RF embedded passives," *IEEE Trans. Microw. Theory Techn.*, vol. 54, no. 5, pp. 1961–1968, May 2006.
- [27] H. Hu, K. Yang, K. L. Wu, and W. Y. Yin, "Quasi-static derived physically expressive circuit model for lossy integrated RF passives," *IEEE Trans. Microw. Theory Techn.*, vol. 56, no. 8, pp. 1954–1961, Aug. 2008.
- [28] Y. Dou and K.-L. Wu, "Direct mesh-based model order reduction of PEEC model for quasi-static circuit problems," *IEEE Trans. Microw. Theory Techn.*, vol. 64, no. 8, pp. 2409–2422, Aug. 2016.
- [29] Y. Dou and K.-L. Wu, "A passive PEEC-based micromodeling circuit for high-speed interconnection problems," *IEEE Trans. Microw. Theory Techn.*, vol. 66, no. 3, pp. 1201–1214, Mar. 2018.
- [30] B. Gustavsen and A. Semlyen, "Enforcing passivity for admittance matrices approximated by rational functions," *IEEE Trans. Power Syst.*, vol. 16, no. 1, pp. 97–104, Feb. 2001.
- [31] S. Grivet-Talocia, "Passivity enforcement via perturbation of Hamiltonian matrices," *IEEE Trans. Circuits Syst. I, Reg. Papers*, vol. 51, no. 9, pp. 1755–1769, Sep. 2004.
- [32] Y. Dou and K.-L. Wu, "Acceleration of a physically derived micro-modeling circuit for packaging problems using graphics processing units," in *IEEE MTT-S Int. Microw. Symp. Dig.*, Honolulu, HI, USA, Jun. 2017, pp. 1638–1640.
- [33] Y. Dou and K.-L. Wu, "Acceleration of parallel computation for derived micro-modeling circuit by exploiting GPU memory bandwidth limit," in *Proc. IEEE Int. Conf. NEMO*, Seville, Spain, May 2017, pp. 146–148.

- [34] Y. Dou, L. K. Yeung, and K.-L. Wu, "Time-domain analysis of circuits with frequency-dependent elements using a SPICE-like solver," in *Proc. IEEE Elect. Design Adv. Packag. Syst. Symp.*, Nara, Japan, Dec. 2013, pp. 193–196.
- [35] C.-C. Chou, W.-C. Lee, and T.-L. Wu, "A rigorous proof on the radiation resistance in generalized PEEC model," *IEEE Trans. Microw. Theory Techn.*, vol. 64, no. 12, pp. 4091–4097, Dec. 2016.
- [36] J. Stoer and R. Bulirsch, "AMOR: An efficient aggregating based model order reduction method for many-terminal interconnect circuits," in *Introduction to Numerical Analysis*, 2nd ed. New York, NY, USA: Springer, 1993, pp. 40–42.
- [37] W. T. Beyene and C. Yuan, "An accurate transient analysis of high-speed package interconnects using convolution technique," *Analog Integr. Circuits Signal Process.*, vol. 35, pp. 107–120, May 2003.
- [38] J.-S. Hong, "Lowpass and bandpass filters," in *Microstrip Filters for RF/Microwave Applications*, 2nd ed. Hoboken, NJ, USA: Wiley, 2011, pp. 128–132.
- [39] A. E. Ruehli, "Equivalent circuit models for three-dimensional multi-conductor systems," *IEEE Trans. Microw. Theory Techn.*, vol. 22, no. 3, pp. 216–221, Mar. 1974.



Yuhang Dou (S'13) received the B.S. degree in electronic engineering from the Nanjing University of Science and Technology, Nanjing, China, in 2012. She is currently pursuing the Ph.D. degree at the Chinese University of Hong Kong, Hong Kong.

Her current research interests include physics-based circuit-domain modeling methods for radiation problems and signal integrity (SI) analysis of high-speed large-scale interconnection and packaging problems.

Ms. Dou was a recipient of First Runner Up awards of both the 2015 and 2018 IEEE Hong Kong AP/MTT Postgraduate Conference.



Ke-Li Wu (M'90–SM'96–F'11) received the B.S. and M.Eng. degrees from the Nanjing University of Science and Technology, Nanjing, China, in 1982 and 1985, respectively, and the Ph.D. degree from Laval University, Quebec, QC, Canada, in 1989.

From 1989 to 1993, he was a Research Engineer with McMaster University, Hamilton, ON, Canada. In 1993, he joined the Corporate Research and Development Division, Honeywell Aerospace, Cambridge, ON, Canada, where he was a Principal Member of Technical Staff.

Since 1999, he has been with The Chinese University of Hong Kong, Hong Kong, where he is currently a Professor and the Director of the Radio Frequency Radiation Research Laboratory. His current research interests include electromagnetic (EM)-based circuit-domain modeling of high-speed interconnections, robot automatic tuning of microwave filters, decoupling techniques of multi-in multi-out (MIMO) antennas, and Internet-of-Things technologies.

Dr. Wu is a member of the IEEE MTT-8 Subcommittee. He was a recipient of the 1998 COM DEV Achievement Award and the Asia-Pacific Microwave Conference Prize in 2008 and 2012, respectively. He serves as a TPC member for many prestigious international conferences. He was an Associate Editor of the IEEE TRANSACTIONS ON MICROWAVE THEORY AND TECHNIQUES from 2006 to 2009.